JOURNAL OF SPACECRAFT AND ROCKETS
Vol. 44, No. 4, July–August 2007

Thermal Design and Analysis for Battery Module for a Remote Sensing Satellite

A. Megahed*
National Authority for Remote Sensing and Space Sciences, Cairo, Egypt 11769
and
A. El-Dib†
Cairo University, Giza, Egypt 12316

DOI: 10.2514/1.19355

Onboard satellite batteries are used for short duration power requirements, such as from the time the satellite is launched until solar panels are deployed and operational. In addition, a battery is needed to supply all the power during periods of eclipse. Proper thermal design and management of a satellite battery is essential for its long life and better performance. The goal of the present work is to estimate thermal behavior of the Ni–Cd battery for a remote-sensing satellite. After the definition of on-orbit battery temperature requirements, charge and discharge cycles are presented for assessment of heat generated by the Ni–Cd battery. A thermal model that simulates the battery module onboard the satellite during its nominal orbit is developed using I-DEAS TMG thermal analysis software. Transient temperature predictions have been obtained on the battery module for the two expected design orbit environments. Analysis results are used to help in the design of a passive thermal control system to maintain acceptable temperature ranges for the battery. Parametric studies are performed in an attempt to determine the optimum passive thermal control hardware. Comparing these results with thermal requirements and constraints of the battery module, the final thermal design is obtained.

Nomenclature

A	=	radiating surface area, m^2
C	=	thermal capacitance, W/K
c	=	specific heat, $J/(kg \cdot K)$
E	=	cell voltage, V
E_{oc}	=	cell open circuit voltage, V
F	=	view factor, dimensionless
I	=	cell current, A
i	=	orbit inclination, degree
K	=	conductive conductance, W/K
k	=	thermal conductivity, $W/(m \cdot K)$
m	=	mass, kg
Q	=	heat generation rate, W
q	=	incident heat flux, W/m^2
T	=	temperature, K
t	=	time, s
α_s	=	solar absorptance, dimensionless
β	=	beta angle
Δt	=	integration time step, s
δ_S	=	declination of the sun, degree
ε	=	emittance, dimensionless
η	=	cell charge efficiency, dimensionless
ρ	=	density, kg/m^3
σ	=	Stephan–Boltzmann constant, $W/m^2 \cdot K^4$
Ω	=	right ascension of the ascending node
Ω_S	=	right ascension of the sun

Subscripts

i, j	=	ith and jth element
n	=	current iteration value

Superscripts

A	=	albedo
E	=	Earth
S	=	solar

I. Introduction

IN ANY satellite power subsystem that uses solar energy, the storage battery is the main source of continuous power, because it is called on to respond to peak and eclipse demands of power depending upon the satellite orbit. The Ni–Cd battery has been the most common space battery since the 1970s. Starting in the early 1980s, there has been renewed interest in employing microsatellites in the scientific, commercial, and military markets, as miniaturized components technology has permitted sophisticated payloads to be fitted into smaller volumes requiring less power. Batteries have special requirements that must be taken into consideration during microsatellite thermal design. Temperature and temperature uniformity are important factors for obtaining optimum performance from the satellite battery module. All the cells in the battery module should operate within the optimum temperature range. In addition, the cells need to be operated at uniform temperatures because uneven temperature distribution in the module leads to different charge/discharge behavior, which, in turn, leads to an electrically unbalanced module and reduced cell performance. Battery specifications require an operating temperature range from 0 to 20°C, which is considered the optimum, and a platform temperature difference, specified at <5°C [1].

Some general aspects of the thermal design and a detailed analysis of the battery and its compartment in the China/Brazil Earth Resources Satellite are presented by Muroaka et al. [2]. The battery compartment is analyzed, using mathematical modeling, to calculate the radiator area and heater power consumption. The battery internal temperature difference is estimated, also using mathematical

Presented as Paper 5610 at the 3rd International Energy Conversion Engineering Conference and Exhibit, San Francisco, CA, 15–18 August 2005; received 5 August 2005; revision received 18 December 2005; accepted for publication 19 December 2005.

*Researcher Assistant, Space Department.
†Professor, Faculty of Engineering, Mechanical Power Department.

modeling, to verify the cells package design. The thermal package developed was used to create the thermal model where the temperature distributions are predicted by a thermal analyzer based on finite differences. De Biasi and Galantini [3] discussed severe constrains imposed on the low Earth orbit operation of the SAX spacecraft batteries and the battery thermal control to guarantee the required performance over the mission. The SAX batteries and their management are based on experimental and theoretical data on Ni–Cd cells behavior with respect to temperature and life dependence. The characteristics of the SAX battery and the relevant management are described. The onboard performance data after accomplishment of the lifetime (26 months) are presented and discussed. A thermal sensitivity analysis was performed for a satellite battery by Suresha et al. [4]. A transient thermal sensitivity is studied for cells that are subjected to conductive heat transfer within themselves and radiative heat transfer with the surrounding environment, including solar heat radiation. Comparison of sensitivities revealed that battery temperature is sensitive to its power dissipation during the beginning of life of the satellite. Moffitt [5] addresses thermal modeling used during the design and analysis of the Combat Sentinel Satellite (CSSAT).

In this paper, a thermal model is developed, using I-DEAS TMG thermal analysis software, to simulate the on-orbit transient thermal response of the Ni–Cd battery and to define the maximum temperature difference across the cells at the given design and operation conditions. The objective is to design a passive thermal control system to maintain acceptable temperature ranges for the battery and to find the main keys that affect battery temperature. This simulation considered two "worst case design" orbit configurations, anticipated to result in the worst case hot and cold extremes. Then a thermal analysis including a parametric study is performed in an attempt to determine the optimum passive thermal control hardware. The following parameters have been studied: the emittance of the battery module, the use of multilayer insulation on the battery module, and improvement of the conductance between the battery module and the satellite structure. Finally comparing these results with battery thermal requirements it is concluded that the passive thermal design is feasible from a thermal point of view to maintain battery temperature within required limits.

II. Mathematical Modeling of Cell Heat Generation

According to the analysis of Montalenti and Stangerup [6], the heat generation rate within a cell is assumed to be uniform; hence the heat generation rate per unit volume of the cell can be written as

$$Q = I\left(E_{oc} - E - T\frac{dE_{oc}}{dT}\right) \tag{1}$$

during discharge, and

$$Q = I\left[\left(E - E_{oc} - T\frac{dE_{oc}}{dT}\right)\eta\right] \tag{2}$$

during charge because all the power is not converted into chemical energy. Macdonald and Challingsworth [7] had shown that the open circuit voltage can be considered constant over the optimum operating temperature range of Ni–Cd cells (0–20°C). Vaidyanathan and Rao [8] calculated the open circuit voltage by measuring heat rates during charge and discharge. The experimental value is 1.461 V.

Table 1 Parameter values for model calculation

Parameter	Value
Capacity	8 Ah
Depth of discharge	25%
I	2 A
E_{oc}	1.461 V
η	0.8

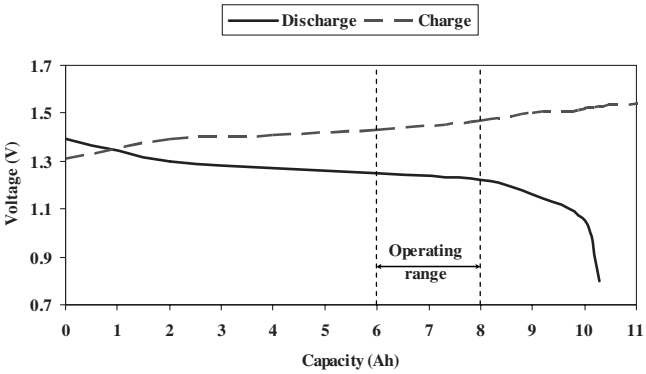

Fig. 1 Cell voltage during charge/discharge cycles.

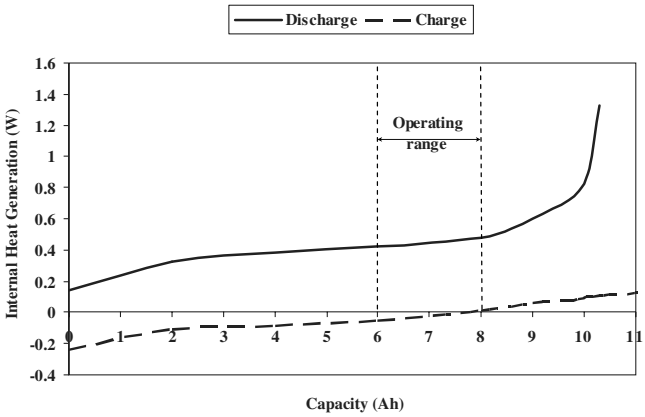

Fig. 2 Internal heat generation during charge and discharge.

The heat capacity and mass of the cell are average values based on the cell components. For the cell considered here, $m = 0.66$ kg, $c = 380$ J/(kg · K), and $k = 10.2$ W/m · K. Other simulation parameters are given in Table 1.

Figure 1 shows the values of both the charge and discharge cycles plotted against the cell capacity. The term "capacity" is frequently used when discussing charging and discharging rates of cells. This term is numerically equivalent to the rated capacity of a cell.

The values of charge and discharge cycles allow accurate calculation of cell heat generation under known load conditions. The heat generation rate as a function of time is given for the same simulations in Fig. 2. This figure demonstrates that the cell is endothermic during more than half of the charge period followed by exothermic reaction as the cell nears full charge. This transition into exothermic occurs at a voltage of 1.461 V. The discharge is exothermic during the entire discharge period. The heat generation rate increases dramatically near the end of discharge because of the decrease of the discharge voltage.

Cells inside the battery module have a prismatic design, and packaged efficiently. This means that the battery can be stored on the satellite in a compact form. The satellite battery module under study consists of 22 cells, the number of which depends upon bus voltage requirements and output voltage of the individual cells. The cells are divided into six cell stacks as shown in Fig. 3.

A cell stack is a configuration of several individual cells. Each cell stack is a configuration of three or four individual cells. The cell stacks would be connected electrically in parallel but thermally in series. The cells are mounted onto a 5 mm thick aluminum plate.

III. Satellite Thermal Model

The satellite thermal model includes an estimate of the temperature changes during charging/discharging of the Ni–Cd cell in the thermal environment of the satellite, which in turn affects the battery charge/discharge characteristics. The satellite under study is a

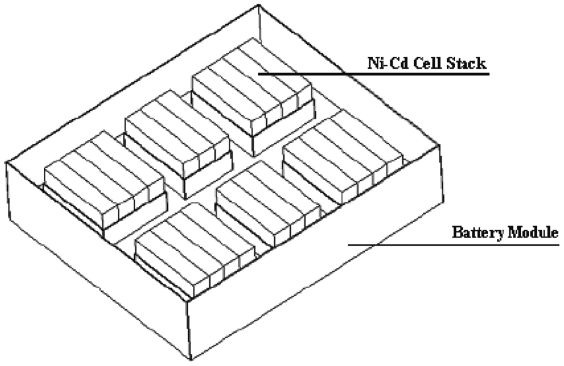

Fig. 3 Three dimensional view of the battery module.

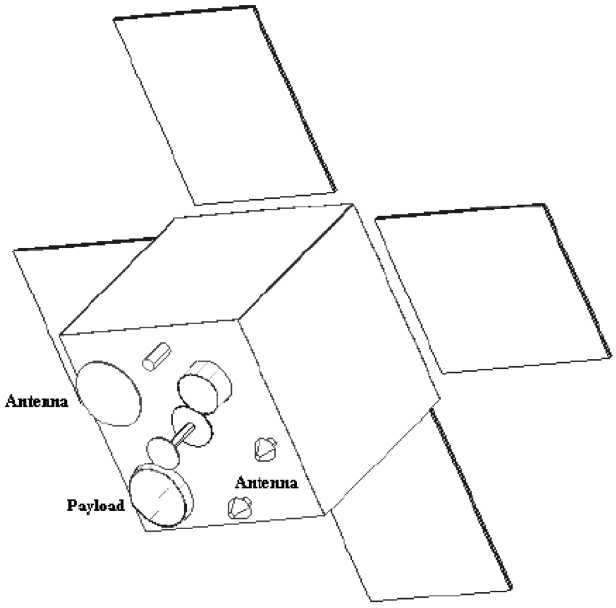

Fig. 4 Satellite main view.

remote-sensing satellite and instruments provide low-cost, multipurpose, land remote-sensing data for Earth. The satellite has five years of lifetime and carries onboard an optoelectronic scanner payload allowing imaging of Earth. Therefore the satellite is oriented in the orbital coordinate system by the longitudinal axis pointed to Earth. The thermal design of this satellite is limited by the low mass requirement. Because of this limitation, an active thermal subsystem cannot be applied as it results in increasing of both satellite mass and power requirements, which are both limited in this mission. By designing a passive thermal system, the complexity of a satellite is greatly reduced, and the limited resources available on small satellites can be better used for payload functions.

Figure 4 shows the deployed configuration of the studied satellite. The satellite is shaped as a rectangular structure with the dimensions of $640 \times 640 \times 680$ mm. The main carrying structure consists of modules and two lower and upper mounting plates. Heat shields are installed on satellite structure to protect the internal subsystems from the space environment which includes sunlight and other radiations. The assembled body of the satellite has the modules stacked in a cubic block with the lower and upper plates secured by studs. The module on the bottom holds the computer. In the next module will be the transmitter electronics and above it the attitude control. The middle module will hold the power regulating module and the battery in the top. The solar arrays are fixed to the outside of this aluminum box by means of rotation mechanisms, which deploy after the separation of the satellite from the launch vehicle.

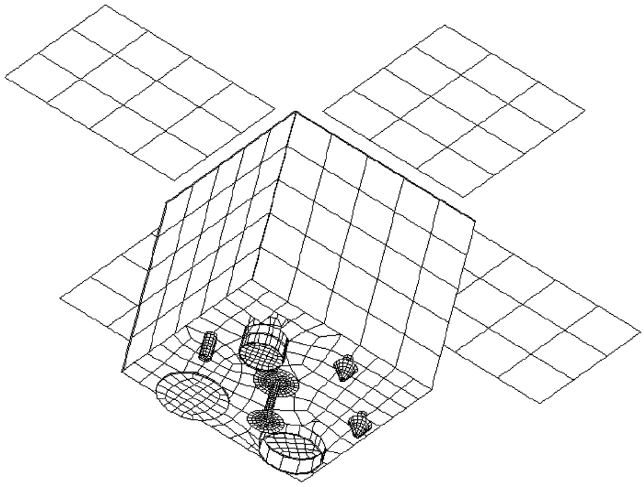

Fig. 5 The whole satellite after meshing.

The geometrical math model (GMM) of the satellite is constructed using I-DEAS TMG. The model consists of a simple representation of the satellite and the payload. It is constructed using rectangular, circular, and cylindrical surface elements, and each surface is assigned the appropriate solar absorptance and emittance. To simulate the physical properties of each component, several materials have been used. Material for all elements is aluminum 2024-Tx with ($k = 120$ W/m $\cdot$ K) ($c = 936$ J/kg $\cdot$ K) ($\rho =$ 2769 kg/m^3) except for the payload which is titanium alloys ($k = 7$ W/m $\cdot$ K) ($c = 540$ J/kg $\cdot$ K) ($\rho = 4430$ kg/m^3). Because the satellite has limited power resources, all the exterior surfaces (heat shields, upper, and lower mounting plate) are selected to be black coated. On the interior of the satellite, it is not desired to exchange energy with the exterior surfaces, thus white paint is used. Table 2 gives the values at the beginning of life (BOL) and end of life (EOL) thermooptical properties of these two coatings.

Each of the satellite components is modeled as a thin shell mesh. The element chosen from the I-DEAS TMG library is a linear quadrilateral thin shell element. Many different elements are created on all surfaces, each one having a different thickness. When the volume is meshed, shell elements are used with a thickness chosen to result in approximately the same mass of the structure. The control volume's computational domain consists of 7098 elements with 9216 nodes. The rotation mechanisms are excluded from the finite element meshing for simplification. Thermal couplings are created between the solar arrays and the upper mounting plate, in the thermal math model (TMM), to simulate the conductive links between them. The satellite is shown in Fig. 5 after meshing.

The extreme environments encountered by the satellite throughout the whole mission drive the thermal design of the battery module. This is defined by setting the external heat radiations and beta angle (β). The β angle of an orbit is the minimum angle measured from the solar vector to the orbit plane. The β angle, together with altitude, primarily characterizes the Earth-shadowing time periods of

Table 2 Thermooptical properties of the coatings applied on the components

Coating	Emittance, ε		Solar absorptance, α_s	
	BOL	EOL, 5 yr	BOL	EOL, 5 yr
CHEMGLAZE black paint Z306	0.91	0.84	0.96	0.96
CATALAC white paint	0.9		0.24	

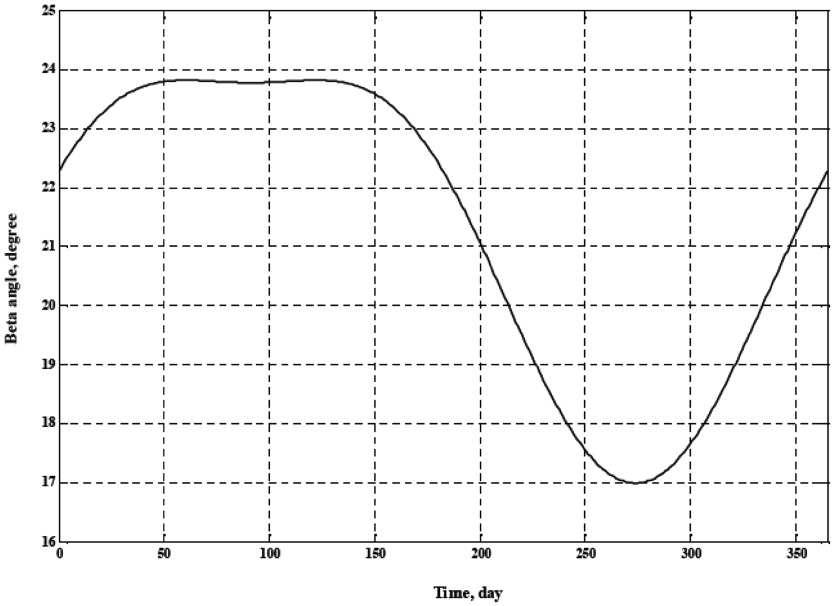

Fig. 6 β angle history for sun-synchronous orbit, 668 km altitude.

missions in orbit. For low β angle orbits, the satellite will experience the maximum Earth shadowing on every orbit. These low β orbits are termed "cold" orbits because they have the lowest average solar heat loading. For high β angle orbits, the satellite may experience little or no Earth shadowing. These higher β angles are termed "hot" orbits because they have the highest average solar heat loading. To prove the satellite's ability to fly in a specified orbit, the entire range of possible β angles must be studied. The satellite orbits Earth at an altitude of 668 km in a sun-synchronous polar orbit with an inclination angle of 98 deg and local time of descending node 10 h 30 min. Calculations are then made to bracket expected β angles. The β angle is defined mathematically as [9]:

$$\beta = \sin^{-1}[\cos\delta_s \cdot \sin i \cdot \sin(\Omega - \Omega_s) + \sin\delta_s \cdot \cos i] \qquad (3)$$

Because of a change in the sun's declination over the year, from 23.45 to -23.45 deg, the β angle is not constant but varies over a small range. The β angle history during 1 year is shown in Fig. 6. For $\beta = 23.7$ deg, which occurs during winter solstice, the satellite spends more time in the sun, thereby increasing the orbit average solar load. On the other hand for $\beta = 17$ deg, which occurs during summer solstice, the solar radiation decreases with eclipse time and albedo.

IV. Analysis Cases

Two orbit configurations will be analyzed, which are intended to represent the worst hot and cold cases. Direct solar radiation, the largest orbital heat load, is the primary concern when classifying orbits according to their thermal characteristics. Orbit 1, which represents hot operating case conditions, includes maximum solar radiation at the highest β angle, maximum Earth infrared (IR) and albedo radiations, and maximum (end of life) solar absorptance on the external surfaces. Orbit 2, which represents cold operating case conditions, includes minimum solar loads at the lowest β angle, minimum Earth IR and albedo radiations, and minimum (beginning of life) solar absorptance. The orbital parameters for both cases are listed in Table 3.

Table 3 Thermal design orbital parameters

Parameter	Orbit 1	Orbit 2
β angle	23.7 deg	17 deg
Solar declination	-23.45 deg	23.45 deg
Orbital period, s	5880	5880
Solar radiation, W/m^2	1400	1310
Albedo factor, dimensionless	0.42	0.34
Earth radiation, W/m^2	233.6	208.3

Running GMM using I-DEAS TMG is then used to calculate the radiation interchange factors between all surfaces. The GMM is then placed mathematically into the proper orbit and attitude. Solar, Earth IR, and albedo heat loads absorbed on each surface were calculated for 50 points (7.2 deg intervals) around the orbit for both hot and cold cases. A sample orbit plot is shown in Fig. 7.

The satellite under study has an average operational load of approximately 60 W. Time-dependent heat load is synchronized for each cell to coincide with the satellite entering and leaving Earth eclipse and to simulate charge and discharge processes. For the satellite under study, it spends 36% of the orbital period (about 35 min) during eclipse time followed by about 64% (about 62 min) during sunlight. Therefore the battery discharges for about 35 min during eclipse followed by charging for about 62 min during sunlight. But for the satellite orientation shown in Fig. 8, when the satellite emerges from eclipse into sunlight, the battery will not start charging because at this point the cell side of the solar array faces the sun. At point a, the battery starts charging until the satellite reaches point b. At this point, the battery is in the discharging mode until it reaches point a and the cycle starts again. Therefore the battery scenario will be that of charging for 45 min followed by 45 min of discharging.

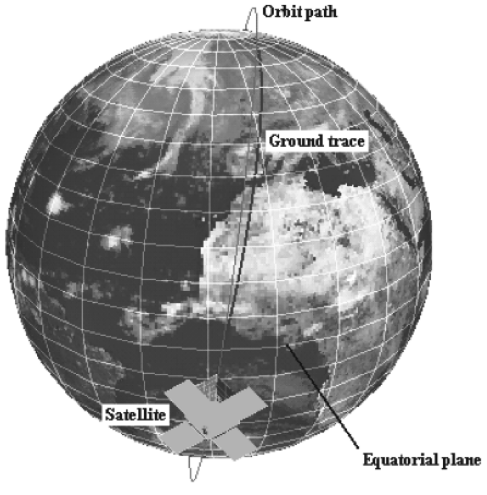

Fig. 7 The satellite as it appears from the sun during orbit 1.

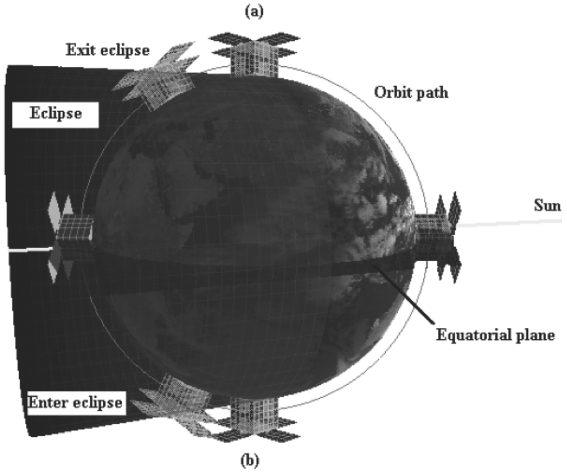

Fig. 8 Different satellite positions in orbit with regard to the sun.

V. Modeling Parameters

Heat fluxes incident on each element of the satellite depend on many parameters, such as position of satellite in orbit, satellite attitude in its current position, relative positions of the sun and Earth, eclipse time, and satellite geometry. Using these heat fluxes, in addition to the operational load, as transient boundary conditions for heat transfer equation, and solving it, the temperature distribution variations of each element are obtained. For the purposes of analysis, the element may be considered isothermal and uniformly radiated to elements j. The heat balance equation for a transient run to be solved iteratively at iteration $n + 1$ and time $t + \Delta t$ for element i can be cast in the form [10]

$$\frac{C_{i,t}(T_{i,t+\Delta t,n+1} - T_{i,t})}{\Delta t} = Q_{i,t+\Delta t}(t) + \left[\alpha_s A^S q^S_{i,t+\Delta t}(t) + \alpha_s A^A q^A_{i,t+\Delta t}(t) + \varepsilon A^E q^E_{i,t+\Delta t}(t)\right]_i - \sigma\varepsilon_i \sum_{j=1}^{N} F_{ij} A_i \left(T^4_{j,t+\Delta t,n+1} - T^4_{i,t+\Delta t,n+}\right) - \sum_{j=1}^{N} K_{ij}(T_{j,t+\Delta t,n+} - T_{i,t+\Delta t,n+}) \quad (4)$$

In the above equation, the term on the left-hand side shows the thermal capacitance of the element. The first term on the right-hand side refers to operational load, the second term is the net external radiant flux absorbed, the third term in the same side is the net radiation rejected, whereas the last term is the internal conduction.

The I-DEAS TMG software uses a finite difference method to solve the heat balance equation and to get the temperature distribution in the model. The backward method is used to solve Eq. (4). In particular, it is most effective for this model where the minimum element time constant is small compared with the solution interval. In addition, it is an accurate method under the conditions of rapid temperature change. Newton's method used to solve the nonlinear system of Eq. (4) for temperatures of n elements [11]. The equations are placed into the matrix format. This solution algorithm is in general much faster than the Jacobi method, particularly for ill-conditioned linear problems. The iteration limit is the maximum number of iterations performed to solve the matrix per time step. If this limit is exceeded, the solver will pass to the next time step. The convergence criterion lets the solving module determine when the matrix is solved. The model is solved by choosing values for the parameters shown in Table 4.

Table 4 Values of modeling parameters

Parameter	Value
Capacity	8 Ah
Depth of discharge	25%
I	2 A
E_{oc}	1.461 V
η	0.8

VI. Transient Results

Figures 9 and 10 show the temperature variations of the maximum and minimum cell temperatures inside the battery module versus time for both orbits 1 and 2, respectively. The results have been computed on 20 orbits to check the stability of the solution. For simulations of both design cases, the emittance of the battery module is fixed at 0.9 and the thermal contact resistance value used is 20°C/W. In these figures, the temperature variation is presented for the last orbit only. Each figure shows two graphs of cells having maximum and minimum temperatures inside the module. The temperature difference between these two graphs presents the maximum temperature difference between cells at a time. In orbit 1, Fig. 9, the temperature of the battery module does not exceed its optimum operating temperature range (17.4 to 19.5°C). In orbit 2, Fig. 10, the temperature of the battery module is also within the allowable temperature range (14.8 to 16.2°C). The maximum temperature difference across the cells is examined for each of the two cases.

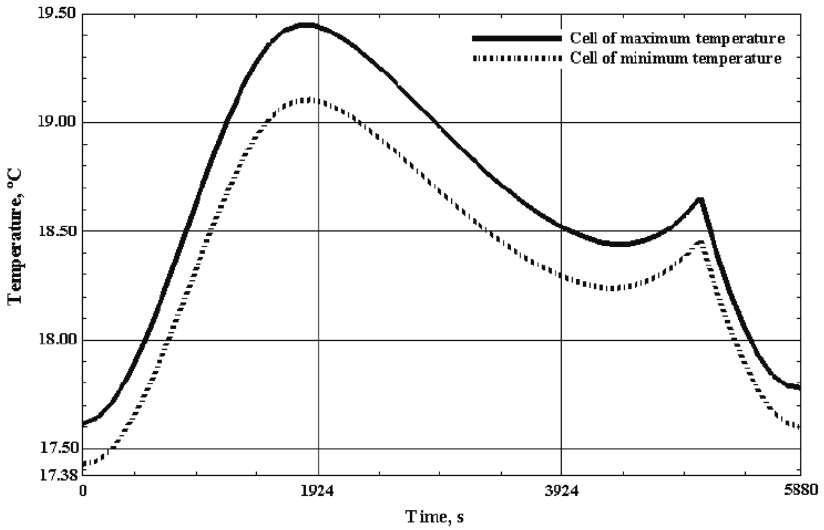

Fig. 9 Temperature variations of cells having maximum and minimum temperatures during orbit 1.

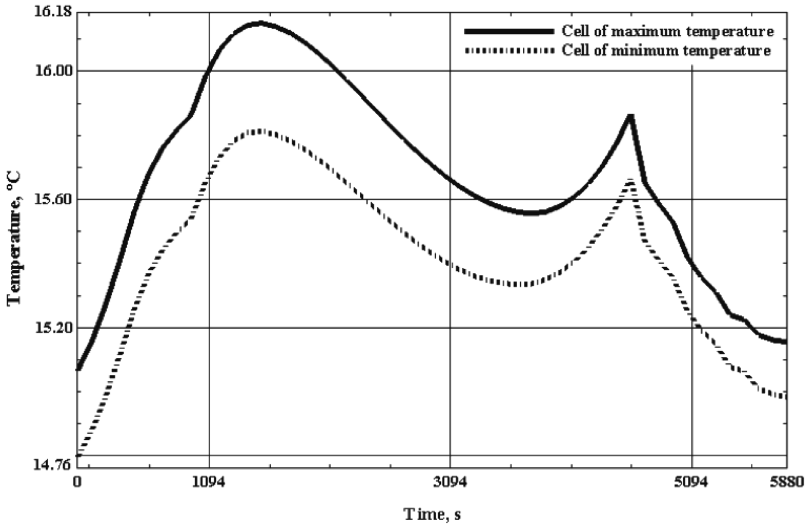

Fig. 10 Temperature variations of cells having maximum and minimum temperatures during orbit 2.

These figures show that the maximum temperature difference is 0.4°C for both cases. The maximum temperature difference between the cells did not exceed the maximum allowable temperature difference (5°C). Compared with thermal requirements it is small and effectively negligible.

The best techniques to reduce the temperature of the battery passively are to apply a high emissive coating such as black paint or to use multilayer insulation (MLI) on the battery sides facing the heat shield facing the sun, and improve conductance through the satellite structure. To determine the best passive thermal control hardware to be applied to the battery module, the following parameters have been parametrically studied: the emittance of the battery module, improving the conductance between the battery module and the satellite structure, and the use of MLI on the battery module.

A. Influence of Battery Emittance

For simulations of both design cases, the emittance of the battery module is fixed at 0.9. Three different values of emittance for the battery have been tried. Table 5 gives the exact values of the maximum and minimum temperatures of the battery module for each case. As one can see in Table 5, when the emittance of the battery is increased, its maximum and temperature range are reduced, but in relatively small proportions. Therefore the emittance of the coating applied on the battery should be emissive as high as possible ($\varepsilon \geq 0.9$).

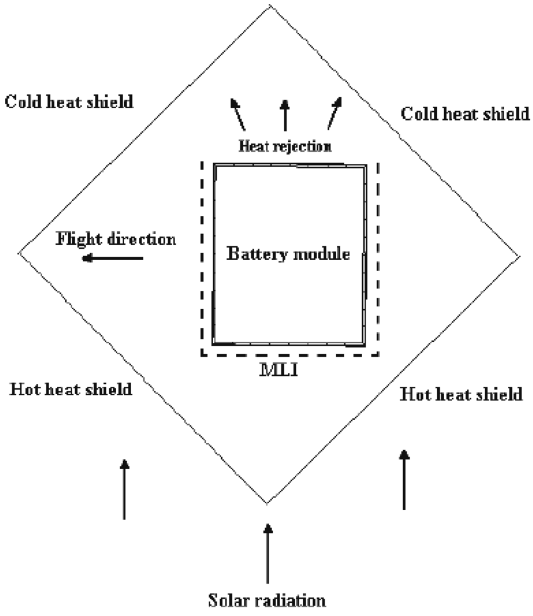

Fig. 11 Battery module sides facing the heat shields.

Table 5 Influence of emittance on the battery temperature

Emittance	Orbit 1		Orbit 2	
	Minimum temperature, °C	Maximum temperature, °C	Minimum temperature, °C	Maximum temperature, °C
0.9	17.40	19.5	14.80	16.20
0.92	17.92	19.04	14.37	15.66
0.94	16.38	19.62	13.83	15.18

Table 6 Influence of thermal contact resistance on the battery temperature

Contact resistance, °C/W	Orbit 1	
	Minimum temperature, °C	Maximum temperature, °C
20	17.40	19.5
15	17.29	19.42
10	17.20	19.35

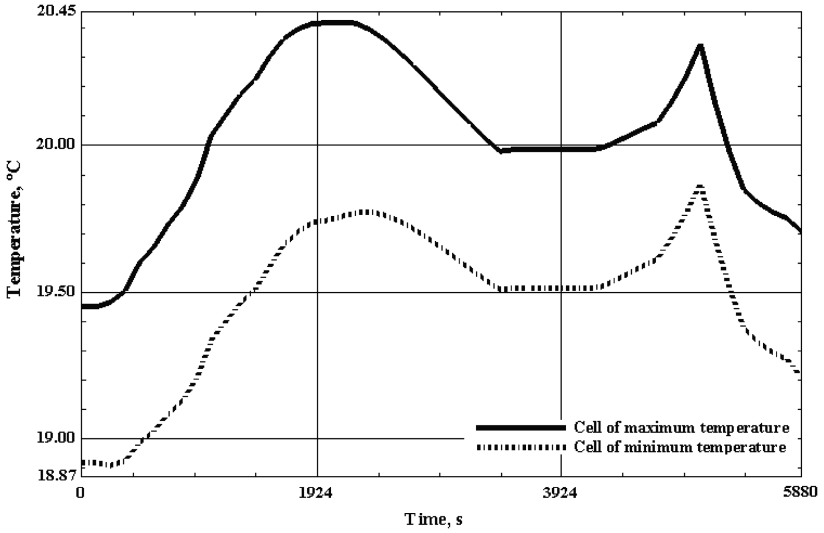

Fig. 12 Temperature variations of cells having maximum and minimum temperatures during orbit 1 when battery module is partially covered by MLI.

B. Sensitivity of the Model to the Conductance Between the Battery Module and the Satellite Structure

The heat path between the satellite structure and the battery module is investigated. Mantelli and Yovanovich [12] determined experimentally the overall thermal resistances of satellite bolted joints. This work examined the effect of applied torque, washer material, washer surface finish, and bolt material on the overall thermal contact resistance. They showed that the overall thermal contact resistance of aluminum washers varies from 10 to 20°C/W. This work was used toward the First Data Collection Brazilian Satellite (SCDI), which was launched 9 February 1993. Table 6 presents the results of the battery average temperature with respect to different values of contact resistance for the hot case. Comparing these results with those in Table 5, the heat path between the battery module and the satellite structure does not have a significant impact on the battery temperature.

C. Sensitivity of the Battery Module to the MLI

Because heat shields are directly exposed to the sun, they will have to withstand the solar heat load throughout the life of the satellite. Moreover because there is a radiant path between the heat shields and the battery, the temperatures of the shields have a direct impact on the temperature of the battery. What is tried is to insulate the battery sides from facing the heat shield exposed to the sun as shown in Fig. 11. In addition, the battery emittance is increased to be 0.94, whereas the thermal contact resistance is decreased to be 10°C/W. With such modifications, it is possible to decrease the radiative conductance between the hot heat shields and the battery, thus decreasing the temperature of the battery. On the other hand, setting the emittance of the battery module side facing the cold heat shields to the maximum value and setting the thermal contact resistance to the minimum value will improve heat rejection. The result with MLI is that the battery overheats. Figure 12 shows the temperature variation of the battery, for the hot case, when the battery is partially covered by MLI.

VII. Conclusions

An on-orbit transient thermal analysis is developed to analyze the temperature of the Ni–Cd battery module for a remote-sensing satellite. The results show that the passive thermal control system is sufficiently designed to withstand the worst design cases, and therefore it will be able to keep the battery module within the required operational temperature range. Also the battery module will not experience high temperature difference between cells during the mission. Increasing battery module emittance results in decreasing its temperature, whereas decreasing thermal contact resistance between the battery module and satellite structure has no significant effect. Covering the battery module partially by multilayer insulation will lead to undesirable results. The temperature of the battery module will exceed the allowable operating temperature range.

Acknowledgments

A. Megahed is grateful to Yu. Petrov and T. Taranova, Department of Spacecraft Thermal Design, Yuzhnoye Design Office, Ukraine, for their constant encouragement for this work.

References

[1] Karam, R. D., *Satellite Thermal Control for System Engineer*, Progress in Astronautics and Aeronautics Series, AIAA, New York, 1998, pp. 132–135.

[2] Muroaka, I., Leite, R. M. G., and Bastos, J. L. F., "Thermal Design Concept of China Brazil Earth Resources Satellite," *Proceedings of the Twenty-First International Conference on Environment Systems*, Society of Automotive Engineers Technical Paper Series, 1991, pp. 1–9.

[3] De Biasi, A., and Galantini, P., "The Ni–Cd Battery Management in LEO Operation: The SAX Experience and In Flight Data," *Proceedings of the Fifth European Space Power Conference*, ESA Publications Division, Noordwijk, The Netherlands, 1998.

[4] Suresha, S., Gupta, S. C., and Katti, R. A., "Thermal Sensitivity of Spacecraft Battery," *Journal of Spacecraft and Rockets*, Vol. 34, No. 3, 1997, pp. 384–390.

[5] Moffitt, B. A., "Predictive Thermal Analysis of the Combat Sentinel Satellite," *Proceedings of the 16th Annual AIAA/Utah State University Conference on Small Satellites*, Utah State Univ., Logan, UT, 2002.

[6] Montalenti, P., and Stangerup, P., "Thermal Simulation of NiCd Batteries for Spacecraft," *Journal of Power Sources*, Vol. 2, No. 2, 1977, pp. 147–162.

[7] Macdonald, D. D., and Challingsworth, M. L., "Thermodynamics of Nickel–Cadmium and Nickel–Hydrogen Batteries," *Journal of the Electrochemical Society*, Vol. 140, No. 3, 1993, pp. 606–609.

[8] Vaidyanathan, H., and Rao, G. M., "Electrode Properties and Heat Generation Rate in Ni–Cd, Ni–H2, and Ni–MH Cells," *Proceedings of the Thirty-First Intersociety Energy Conversion Engineering Conference*, Vol. 1, AIAA, Washington, D.C., Oct. 1996, pp. 83–86.

[9] Gilmore, D., *Satellite Thermal Control Handbook*, Aerospace Corp. Press, El Segundo, CA, 1994, pp. 2-18–2-19.

[10] *I-DEAS TMG Reference Manual*, MAYA Heat Transfer Technologies, Ltd., Montreal, Canada, Jan. 2003.

[11] Krishnaprakas, C. K., "Application of Accelerated Iterative Methods for Solution of Thermal Models of Spacecraft," *Journal of Spacecraft and Rockets*, Vol. 32, No. 4, 1995, pp. 608–611.

[12] Mantelli, M. B. H., and Yovanovich, M. M., "Experimental Determination of Overall Thermal Resistances of Satellite Bolted Joints," *Journal of Thermophysics and Heat Transfer*, Vol. 10, No. 1, 1996, pp. 177–179.

I. Vas
Associate Editor